

EXTRINSIC SOURCES OF SCATTER IN THE RICHNESS–MASS RELATION OF GALAXY CLUSTERS

EDUARDO ROZO^{1,2}, ELI RYKOFF³, BENJAMIN KOESTER⁴, BRIAN NORD^{5,7}, HAO-YI WU⁶, AUGUST EVRARD⁵, RISA WECHSLER⁶*Draft version January 19, 2013*

ABSTRACT

Maximizing the utility of upcoming photometric cluster surveys requires a thorough understanding of the richness–mass relation of galaxy clusters. We use Monte Carlo simulations to study the impact of various sources of observational scatter on this relation. Cluster ellipticity, photometric errors, photometric redshift errors, and cluster-to-cluster variations in the properties of red-sequence galaxies contribute negligible noise. Miscentering, however, can be important, and likely contributes to the scatter in the richness–mass relation of galaxy maxBCG clusters at the low mass end, where centering is more difficult. We also investigate the impact of projection effects under several empirically motivated assumptions about cluster environments. Using SDSS data and the maxBCG cluster catalog, we demonstrate that variations in cluster environments can rarely ($\approx 1\% - 5\%$ of the time) result in significant richness boosts. Due to the steepness of the mass/richness function, the corresponding fraction of optically selected clusters that suffer from these projection effects is $\approx 5\% - 15\%$. We expect these numbers to be generic in magnitude, but a precise determination requires detailed, survey-specific modeling.

Subject headings: cosmology: clusters

1. INTRODUCTION

The abundance of galaxy clusters as a function of mass has long been recognized as a powerful cosmological tool (Peebles et al. 1989; Evrard 1989). Clusters are highly complementary to other dark energy experiments (Cunha et al. 2009), and, along with weak lensing tomography, cluster abundances can distinguish between dark energy and modified gravity as the fundamental driver of our Universe’s current phase of accelerating expansion (Shapiro et al. 2010). Unfortunately, cluster mass is not a direct observable, so one is forced instead to compute the abundance of galaxy clusters as a function of observables that correlate with mass. If the observable–mass relation is well understood, one can effectively recover the cosmological information inherent in the halo mass function.

Over the next several years, a variety of large scale photometric surveys such as the Dark Energy Survey (DES)⁸ and the Large Synoptic Survey Telescope (LSST)⁹ are expected to observe large fractions of the sky to extremely faint magnitudes. Using a wide variety of techniques (e.g. Gladders & Yee 2000; Miller et al. 2005; Koester et al. 2007; Dong et al. 2008; Wen et al. 2009a; Milkeraitis et al. 2010; Hao et al. 2010), these surveys will identify hundreds of thousands of clusters out to red-

shift, $z \sim 1$ and beyond, resulting in catalogs of incredible statistical power. To fully realize the promise of such catalogs, however, we must have a detailed understanding of the richness–mass relation of these systems. In particular, we must understand not only what the mean scaling between richness and mass is, but also how individual galaxy clusters scatter about this relation.

In general, we expect there to be two distinct sources of noise which must be characterized, namely *intrinsic* and *extrinsic* scatter. By intrinsic scatter, we mean the fact that the galaxy content of halos of a given mass will randomly vary from halo to halo, even if we could unambiguously identify which galaxies belong to which halo with complete confidence. In this work, we will simply assume that intrinsic scatter can be adequately modeled as Poisson. This Poisson model is found to be a reasonable description of the scatter in the halo occupation distribution of both dark matter halos (Kravtsov et al. 2004) and simulated galaxies (e.g. Berlind et al. 2003; Zheng et al. 2005), and is a key-component of halo model fits of galaxy clustering (e.g. Blake et al. 2008; Zheng et al. 2009; Zehavi et al. 2010; Tinker et al. 2010). We note, however, that recent work suggests the intrinsic scatter may in fact be significantly super-Poisson in the large occupation limit (Boylan-Kolchin et al. 2010; Wetzel & White 2010; Busha et al. 2010). If so, this can only decrease the relative importance of the extrinsic sources of scatter considered here.

Let us turn then to the focus of this paper: extrinsic sources of scatter. In principle, there is a plethora of effects that must be accounted for, such as halo triaxiality, photometric errors, projection effects, etc., so the prospect of such a calibration is truly daunting. In practice, however, not all of these possibilities are necessarily observationally relevant. *The goal of this paper is to identify all sources of extrinsic scatter that are observationally relevant.* Having identified the relevant sources of scatter, we intend to return in a future work to

¹ Einstein Fellow, Department of Astronomy & Astrophysics, The University of Chicago, Chicago, IL 60637.

² Kavli Institute for Cosmological Physics, Chicago, IL 60637.

³ Lawrence Berkeley National Laboratory, Berkeley, CA 94720.

⁴ Department of Astronomy & Astrophysics, The University of Chicago, Chicago, IL 60637.

⁵ Department of Physics, University of Michigan, Ann Arbor, MI 48109.

⁶ Kavli Institute for Particle Astrophysics and Cosmology, Physics Department, Stanford University, Stanford, CA 94305.

⁷ AGEP Fellow, Department of Physics, University of Michigan, Ann Arbor, MI 48109.

⁸ <http://www.darkenergysurvey.org/>

⁹ <http://www.lsst.org/lsst>

the problem of modeling the relevant sources of scatter quantitatively. Note that if a source of extrinsic scatter is negligible relative to Poisson intrinsic scatter, it is also negligible relative to super-Poisson scatter, so our analysis is conservative in that sense.

To identify which sources of measurement noise are observationally relevant we rely on a Monte Carlo approach: using analytic models, we simulate galaxy clusters under a variety of different assumptions about extrinsic sources of noise, and then estimate their richness to determine whether the richness–mass relation was affected at a significant level (where “significant” is quantitatively defined below). While this method lacks the sophistication of N-body simulations, it has the significant advantage of permitting control of every detail of the simulated clusters. More specifically, we can turn on the sources of extrinsic scatter one at a time in order to identify those that are observationally relevant. Moreover, it gives us the ability to very quickly simulate hundreds of thousands of clusters, which is necessary for us to accomplish our goals. We believe this Monte Carlo approach should suffice for our stated goal of identifying relevant sources of scatter, though clearly further work will be required to quantitatively characterize those sources of scatter that are observationally relevant.

This paper is the second in a series of papers that have as their final goal the development of a fully optimized richness estimator that is both qualitatively and quantitatively understood. The first of these papers (Roza et al. 2009, henceforth referred to as paper I) introduced the general matched filter formalism we use to estimate cluster richness, and tuned it to minimize the scatter in X-ray luminosity of galaxy clusters at fixed richness (similar approaches towards richness estimation and cluster finding can be found in Kepner et al. 1999; White & Kochanek 2002; Kochanek et al. 2003; Dong et al. 2008). Here, we identify those sources of extrinsic scatter that can impact the observed richness–mass relation, while a companion paper (paper III) considers various modifications to the richness estimator λ in an effort to further improve the fidelity with which cluster richness traces mass (Rykoff et al. 2010, henceforth referred to as paper III). Our final richness estimator is extremely robust, and we believe is close to being fully optimal for counting red-sequence galaxies from photometric data. We intend to follow these two papers with an additional quantitative study of the sources of extrinsic scatter identified in this work.

The layout of this paper is as follows: in section 2 we quickly review the richness estimator λ from paper I, while section 3 details our method for generating Monte Carlo realizations of galaxy clusters. Section 4 explores a wide variety of extrinsic sources of scatter, and section 5 considers the impact of projections effects on cluster richness for a variety of empirically motivated assumptions about the environment of galaxy clusters. Section 6 summarizes our results. Appendix A details the reasoning behind the definition adopted in the main body of the work as to what constitutes an observationally relevant source of scatter. Unless otherwise stated, all of our calculations assume a fiducial flat Λ CDM cosmology with $h = 0.7$ and $\Omega_m = 0.25$.

2. THE RICHNESS MEASURE λ

We begin by summarizing the algorithm behind the matched filter richness λ originally proposed in paper I. Let i index all galaxies around a putative cluster center, and y_i be a random variable such that $y_i = 1$ if a galaxy is a member of a galaxy clusters, and $y_i = 0$ otherwise. The richness is defined as the total number of cluster galaxies

$$\lambda = \sum_i y_i. \quad (1)$$

Define p_i as the membership probability of galaxy i , so that $P(y_i = 1) = p_i$ and $P(y_i = 0) = 1 - p_i$. The mean and variance of the richness λ are given by

$$\langle \lambda \rangle = \sum_i \langle y_i \rangle = \sum_i p_i \quad (2)$$

$$\text{Var}(\lambda) = \sum_i \text{Var}(y_i) = \sum_i p_i(1 - p_i). \quad (3)$$

If the membership probabilities p_i are known, then equation 2 can be used to define the richness estimator $\hat{\lambda}$ via $\hat{\lambda} = \langle \lambda \rangle$, while equation 3 would correspond to the statistical uncertainty in $\hat{\lambda}$.

Expanding the product in the expression for the variance, we find

$$\text{Var}(\lambda) = \langle \lambda \rangle (1 - \bar{p}) \quad (4)$$

where \bar{p} is the mean membership probability,

$$\bar{p} = \frac{\sum_i p_i^2}{\sum_i p_i} = \frac{1}{\langle \lambda \rangle} \sum_i p_i^2. \quad (5)$$

This implies that as long as the mean membership probability is close to unity, the statistical uncertainty in the richness is significantly smaller than Poisson.

The membership probabilities are estimated as follows: let \mathbf{x} be a vector describing the observable properties of a galaxy (e.g. galaxy color, magnitude, and position). We model the projected galaxy distribution around clusters as a sum $S(\mathbf{x}) = \lambda u(\mathbf{x}|\lambda) + b(\mathbf{x})$, where λ is the number of cluster galaxies, $u(\mathbf{x}|\lambda)$ is the number density profile of cluster galaxies normalized to unity, and $b(\mathbf{x})$ is the density of background (i.e. non-member) galaxies. The probability that a galaxy found near a cluster is actually a cluster member is simply

$$p(\mathbf{x}) = \frac{\lambda u(\mathbf{x}|\lambda)}{\lambda u(\mathbf{x}|\lambda) + b(\mathbf{x})}. \quad (6)$$

Inserting these probabilities back into equation 2 we arrive at

$$\lambda = \sum p(\mathbf{x}|\lambda) = \sum_{R < R_c(\lambda)} \frac{\lambda u(\mathbf{x}|\lambda)}{\lambda u(\mathbf{x}|\lambda) + b(\mathbf{x})}. \quad (7)$$

Equation 7 can be solved for the value of λ , which in turn defines our richness estimator. In principle, the sum should extend over all galaxies. In practice, one needs to add over all galaxies within some cutoff radius R_c and above some luminosity cut L_{cut} , for which we set $R_c = 1$ Mpc and $L_{cut} = 0.2L_*$ unless otherwise noted. The choice of a fixed metric aperture is purely for simplicity. Paper III has a detailed discussion of the impact of the radial aperture on the richness–mass relation, and optimizes the radial aperture so as to minimize the scatter in L_X at fixed richness.

We consider three observable galaxy properties: R , the projected distance from the cluster center; m , the galaxy i -band magnitude; and c , the galaxy $g - r$ color, as appropriate for low redshift galaxy clusters. We adopt a separable filter function

$$u(\mathbf{x}) = [2\pi R \Sigma(R)] \phi(m) G(c) \quad (8)$$

where $\Sigma(R)$ is the two dimensional cluster galaxy density profile, $\phi(m)$ is the cluster luminosity function (expressed in apparent magnitudes), and $G(c)$ is color distribution of cluster galaxies. The pre-factor $2\pi R$ in front of $\Sigma(R)$ accounts for the fact that given $\Sigma(R)$, the radial probability density distribution is $2\pi R \Sigma(R)$. We summarize each of these filters below.

2.1. The Radial Filter

We assume cluster galaxies follow an NFW profile (Navarro et al. 1995). The corresponding two-dimensional surface density profile is (Bartelmann 1996)

$$\Sigma(R) \propto \frac{1}{(R/R_s)^2 - 1} f(R/R_s) \quad (9)$$

where R_s is the characteristic scale radius, and

$$f(x) = 1 - \frac{2}{\sqrt{x^2 - 1}} \tan^{-1} \sqrt{\frac{x-1}{x+1}}. \quad (10)$$

This formula assumes $x > 1$. For $x < 1$, one uses the identity $\tan^{-1}(ix) = i \tanh(x)$. As in paper I, we set $R_s = 0.15 h^{-1} \text{Mpc}$. While the profile is singular as $R \rightarrow 0$, the membership probability remains finite with $p \rightarrow 1$ as $R \rightarrow 0$. The filter $\Sigma(R)$ is normalized to unity within our chosen fixed metric aperture $R_c = 1 \text{ Mpc}$,

$$1 = \int_0^{R_c} dR \, 2\pi R \Sigma(R). \quad (11)$$

2.2. The Luminosity Filter

The luminosity distribution of maxBCG clusters is well represented by a Schechter function (e.g. Hansen et al. 2007), which we write as

$$\phi(m) = C 10^{-0.4(m-m_*)(\alpha+1)} \exp\left(-10^{-0.4(m-m_*)}\right) \quad (12)$$

where $C = 0.4 \ln(10) \phi_*$. The normalization ϕ_* is fixed by requiring that ϕ be normalized to unity above a luminosity cut L_{cut} , which we set to $L_{cut} = 0.2 L_*$. This is fainter than the cut adopted in paper I, but matches the final cut we adopt in paper III. We also set $\alpha = 0.8$, and we calculate m_* using passively evolved stellar population models (see Koester et al. 2007, for details). An accurate polynomial interpolation for $i_{cut}(z)$ is

$$i_{cut} = 19.605 + 2.327x + 0.205x^2 + 0.202x^3 \quad (13)$$

where $x = \ln(1 + \delta_z)$ and $\delta_z = (z - 0.2)/0.2$. This fitting function is accurate at the level of $\Delta i_{cut} = 0.002$ over the redshift range $0.1 \leq z \leq 0.3$.

2.3. The Color Filter

For a color filter, we assume red-sequence galaxies have a Gaussian color distribution with intrinsic dispersion $\sigma_{int} = 0.05 \text{ mag}$. The corresponding color filter, $G(c)$ is

$$G(c|z) = \frac{1}{\sqrt{2\pi}\sigma} \exp\left[-\frac{(c - \langle c|z \rangle)^2}{2\sigma^2}\right], \quad (14)$$

where $c = g - r$ is the color of interest, $\langle c|z \rangle$ is the mean of the Gaussian color distribution of early type galaxies at redshift z , and σ is the width of the distribution. The mean color $\langle c|z \rangle = 0.625 + 3.149z$ was determined by matching maxBCG cluster members to the SDSS LRG (Eisenstein et al. 2001) and MAIN (Strauss et al. 2002) spectroscopic galaxy samples. The net dispersion σ is taken to be the sum in quadrature of the intrinsic color dispersion $\sigma_{int} = 0.05$ and the estimated color error σ_c of each individual galaxy.

2.4. Background Model

The last necessary ingredient for estimating λ is a background model. We assume the background galaxy density is constant in space, so that $b(\mathbf{x}) = 2\pi R \bar{\Sigma}_g(m_i, c)$ where $\bar{\Sigma}_g(m_i, c)$ is the galaxy density as a function of galaxy i -band magnitude and $g - r$ color. In paper III we estimate $\bar{\Sigma}_g$ by binning SDSS galaxies in color-magnitude space using a cloud-in-cell (CIC) algorithm (e.g. Hockney & Eastwood 1981). We use those results to define our background model at every point through linear interpolation. Further details of how the background density model is constructed can be found in paper III. For our purposes, the key is that we have an empirically determined function $\bar{\Sigma}_g(m_i, c)$ that returns the mean galaxy density of the universe as a function of i -band magnitudes and $g - r$ color.

3. METHOD

Our idea is simple: using the filters $\Sigma(R)$, $\Phi(m)$, and $G(g-r)$, we generate Monte Carlo realizations of a single cluster, and measure the scatter in richness. We can then repeat the experiment including an extrinsic source of scatter, and determine whether the newly introduced effects is observationally relevant or not.

We simulate the galaxy density field around a galaxy cluster out to a 3 Mpc radius, comfortably larger than the 1 Mpc aperture used to estimate cluster richness. To generate the galaxy fields, we first select the expectation value $\bar{\lambda}_{in}$ for the number of red sequence galaxies in a cluster within a 1 Mpc radius. Using the radial filter $\Sigma(R)$, we extrapolate in radius to compute the expected number of red sequence galaxies within 3 Mpc, which we label \bar{N}_3 . The number of galaxies assigned to the cluster is a Poisson realization of mean \bar{N}_3 . Each cluster galaxy is assigned a radius, angle, magnitude, and color, by randomly sampling the filters $\Sigma(R)$, $\Phi(m)$, and $G(c)$. The brightest galaxy is always placed at the center of the cluster. If λ_{in} is small, it is possible for no galaxies to be bright enough to pass the magnitude cut. Since observationally we are restricted to systems with at least one bright galaxy, whenever this happens we simply add a central galaxy. Note that means that when $\bar{\lambda}_{in} \rightarrow 1$, we expect large biases in the sampled of detected clusters simply because one misses all systems with no galaxies.

Once cluster galaxies are in place, we use a similar procedure to populate our sky patch with non-cluster galaxies. Given a background model $b(R, m, c)$, we compute the expected number of such galaxies, draw the number of background galaxies from a Poisson distribution of the appropriate mean, and then assign to every galaxy a radius, angle, magnitude, and color using the background filters. Note that the background model used to generate our Monte Carlo simulations need not be the same as the

background model employed to estimate λ . Throughout section 4, however, we will use the density model from section 2.4 both for populating our simulations with non cluster galaxies, and for estimating richness. To convert the observed mean galaxy density from gal/deg^2 to gal/Mpc^2 , we assume a flat Λ CDM cosmology with $\Omega_m = 0.3$ and $h = 0.7$.

Once a patch has been generated as described above, we estimate its richness, which we henceforth refer to as λ_{out} . The richness is estimated as described in section 2. To measure the statistical properties of λ_{out} , we repeat this procedure a minimum of 400 times. When confronted with noisy realizations (e.g. when considering miscentering), we increase the number of samples up to 10,000 realizations (per choice of miscentering parameters). Finally, we emphasize that since $\bar{\lambda}_{in}$ is a deterministic function of the mass (e.g. $\bar{\lambda}_{in} \propto M^\alpha$), holding $\bar{\lambda}_{in}$ constant is equivalent to holding halo mass constant. That is, the scatter we measure is precisely the scatter in richness at fixed mass, $\sigma_{\ln \lambda|M}$. Throughout, we use the word “scatter” to signify the standard deviation of $\ln \lambda_{out}$ at fixed $\bar{\lambda}_{in}$.

It is obvious from the above description that in these Monte Carlo realizations there is no allowance for contamination of the cluster field by correlated galaxies. We address this difficulty in section 5, where we change the background model used to populate cluster fields with non-cluster galaxies. For our purposes, the most relevant result concerning projection effects is that they are rare, but severe. That is, projection effects don’t really broaden the peak of the probability distribution $P(\lambda_{out}|\lambda_{in})$. Rather, they build a small non-gaussian where λ_{out} is much larger than expected. Throughout section 4, we focus exclusively on the central component of the distribution $P(\lambda_{out}|\bar{\lambda}_{in})$.

Using the method described above to generate Monte Carlo realization of galaxy clusters, we can measure the distribution $P(\lambda_{out}|\lambda_{in})$. In most cases, we focus exclusively on the mean and scatter of this distribution. The two obvious questions that can be addressed with such data are: 1) is our richness estimator biased? 2) is the scatter of our richness estimator consistent with Poisson?

Concerning the first question, we emphasize that *biases in our richness estimator are irrelevant*. The richness measure λ is only meant to be interpreted as an observational quantity that scales with mass with little scatter. The scaling of richness with both mass and redshift needs to be empirically calibrated regardless of whether λ_{out} is biased relative to $\bar{\lambda}_{in}$ or not. Thus, biases in $\langle \lambda_{out}|\lambda_{in} \rangle$ are of no practical consequence. It is the scatter in λ_{out} that we are primarily concerned about.

Finally, we need to determine how much extrinsic scatter we can tolerate before the extrinsic scatter becomes observationally relevant, i.e. how far can we deviate from Poisson scatter. Here, we focus on whether the scatter in λ_{out} can be modeled as Poisson for the purposes of the Dark Energy Survey (DES). In appendix A, we demonstrate that differences between the true and predicted scatter of the richness–mass relation are irrelevant so long as these differences are about 5% or less, (i.e. $\Delta\sigma_{\ln \lambda} \lesssim 0.05$). Thus, for this work, we will say that a source of scatter is observationally irrelevant whenever

$$\Delta\sigma_{\ln \lambda} \leq 0.05.^{10}$$

4. SOURCES OF SCATTER FOR THE RICHNESS–MASS RELATION OF GALAXY CLUSTERS

We wish to determine what sources of statistical and/or systematic uncertainty can significantly impact the observed richness–mass relation. The effects we consider are halo triaxiality, cluster-to-cluster scatter in the properties of ridgeline galaxies, photometric errors, photometric redshift errors, and cluster miscentering. Before we proceed, however, we must set a baseline, and determine what the richness–mass relation of galaxy clusters is in the absence of any such additional sources of noise.

4.1. The Intrinsic Scatter of the Richness–Mass Relation

The top panel in Figure 1 shows the distribution of λ_{out} obtained from 10^4 realizations of a cluster with $\bar{\lambda}_{in} = 50$ galaxies. The solid curve is the best-fit Gaussian, and the vertical dotted line is the input richness. Two things are evident from this figure: first, our richness estimator is nearly unbiased, and second, the distribution $P(\lambda_{out}|\bar{\lambda}_{in})$ can be adequately modeled as Poisson. Of course, readers will be quick to note that the actual number of cluster galaxies we place in our 3 Mpc field is itself drawn from a Poisson distribution. Are we engaging in circular reasoning?

The answer is only partially. Consider the process used to create and test the Monte Carlo simulations: given $\bar{\lambda}_{in}$, we draw a Poisson realization for the number of galaxies in the cluster field, in accordance with naive expectation for the *intrinsic* scatter of the richness–mass relation. If the reasoning were circular, the exercise would conclude with this stage. In our simulations, however, we use Poisson statistics to populate a 3 Mpc cluster field with galaxies, we then randomly add background galaxies, and finally, we estimate the richness within a 1 Mpc aperture. This whole procedure must necessarily introduce some amount of measurement error (for instance, λ is not an integer), but it is readily apparent from our results that this extra noise is negligible relative to the expected intrinsic scatter. Thus, the scatter we recover is Poisson both because the intrinsic scatter is Poisson, and because the measurement error associated with estimating richness is negligible, as we had anticipated from equation 3.

The bottom panel in Figure 1 explores the extent to which our conclusions depend on the richness of the cluster under consideration. The figure shows the bias in the mean (diamonds) as well as the deviation from the Poisson expectation for the standard deviation (points with error bars) as a function of the input richness $\bar{\lambda}_{in}$. As we can see, our above conclusions are valid at richnesses $\lambda \gtrsim 15$, though measurement error does become more important with decreasing cluster richness. The bias at low richness is due to the fact that we demand a central galaxy to always be present.

4.2. Halo Triaxiality

¹⁰ To estimate $\sigma_{\ln \lambda}$ for a Poisson distribution, we use 10^5 Poisson realizations and numerically estimate $\sigma_{\ln \lambda}$. As with the real data, if a realization results in no galaxies, we set $\lambda_{out} = 1$ instead.

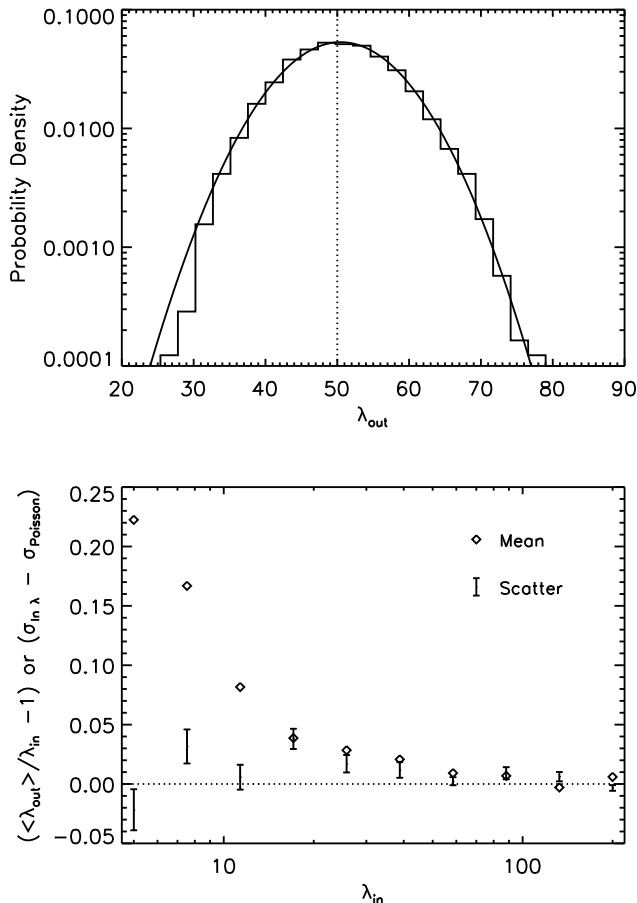


FIG. 1.— *Top panel:* The distribution of the estimated richness λ_{out} for 10^4 independent realizations of a single cluster with $\lambda_{in} = 50$. The distribution has a slight (1%) bias in the mean, and the scatter is very well approximated by Poisson. Note that since the richness–mass relation needs to be empirically calibrated, a bias in the mean is not of importance to us. *Bottom panel:* The first two moments of the $\lambda_{out} - \lambda_{in}$ relation as a function of richness. Diamonds show the bias of our richness estimator $\langle \lambda_{out} \rangle / \lambda_{in} - 1$, while the points with error bars show the deviation $\Delta \sigma_{\ln \lambda_{out}}$ of the observed scatter in $\ln \lambda_{out}$ from the Poisson expectation. For $\lambda_{in} \geq 20$, our richness estimates are slightly biased, and the scatter can be approximated as Poisson.

Halos are known to be triaxial, with halo triaxiality depending on both halo mass and redshift (e.g. Bett et al. 2007; Kasun & Evrard 2005; Knebe & Wießner 2006; Shaw et al. 2006; Allgood et al. 2006; Jing & Suto 2002). This has two important consequences: first, the projected galaxy density of a halo is not circularly symmetric, and second, the amplitude of the density field is itself modulated by the line of sight projection. We explore both effects, beginning with the impact of non-circular symmetry. We modify our simulations as follows: first, we select the minimum projected axis ratio q_{min} that an elliptical cluster can have in our realizations. The projected axis ratio q of each realization is drawn uniformly from the range $[q_{min}, 1]$. While not realistic, this certainly suffices for the purposes of determining whether scatter in the projected ellipticity of a halo can introduce significant scatter in the richness–mass relation. For each mock realization, we draw a different axis ratio q , and randomly place galaxies according to the corresponding elliptical halo profile $u(\rho)$ where ρ is now an elliptical

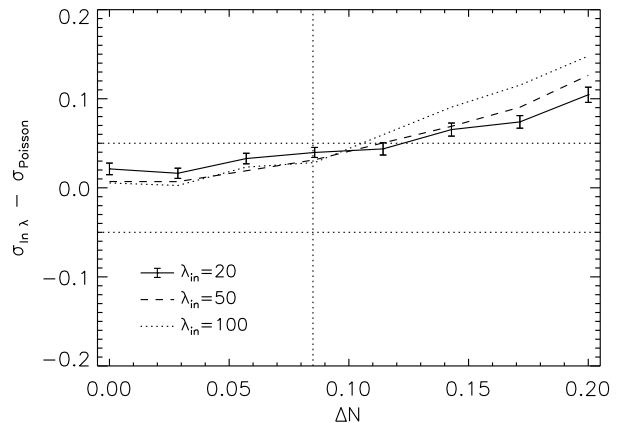


FIG. 2.— Bias and deviation from the Poisson expectation of the scatter of the richness–mass relation as a function of ΔN , the standard deviation of the surface density amplitude for triaxial halos. The vertical dotted line marks a rough estimate for ΔN for triaxial halos. We find halo-triaxiality can increase the scatter of the richness–mass relation by $\Delta \sigma_{\ln \lambda} = 0.04$, which is border-line important. For clarity, we only show error bars for the $\lambda_{in} = 20$ case, but the errors are comparable for the different λ_{in} values.

coordinate, $\rho^2 = x^2 + q^2 y^2$. All other aspects of our simulation remain unchanged.

We find that cluster ellipticity impacts the richness–mass relation only at the $\lesssim 2\%$ level in the mean, and that the scatter can be described as Poisson at comparable accuracy for $q_{min} \geq 0.5$. Consequently, variance in the ellipticity of the galaxy distribution does not significantly impact the richness–mass relation of galaxy clusters. This result emphasizes an important distinction that often gets overlooked: using radial filters is *not* equivalent to assuming spherical symmetry. For instance, lining up galaxies while preserving their radial distribution has no impact on a cluster’s richness as defined in section 2. Thus, it is not surprising that the projected ellipticity of the galaxy distribution of halo has little effect on the richness–mass relation.

We now turn to the line of sight modulation of the amplitude of the galaxy density field. We adopt a simple model of the form

$$\Sigma_{g,cluster}(R) = N \bar{\lambda}_{in} u(R) \quad (15)$$

where $u(R)$ is the cluster profile normalized to unity, and N is a normalization constant that depends on the axis ratios q_1 and q_2 of the triaxial halo and on the line of sight $\hat{\mathbf{n}}$ along which the halo is projected. Given the statistical properties of the triaxial halo population, one can compute the corresponding probability density $P(N)$. However, because our goal is only to determine whether halo triaxiality can significantly impact the scatter of the richness–mass relation, we consider instead a simple Gaussian distribution for N , and explore how the richness–mass relation depends on the standard deviation of N , which we denote ΔN . To estimate a typical value for ΔN , we rely on the results of Rozo et al. (2007a), who computed $N(q_1, q_2, \hat{\mathbf{n}})$ for the case of a triaxial singular isothermal ellipsoid. Assuming the axis q_1 and q_2 are drawn from a uniform distribution $q_1 \in [0.5, 1]$ and $q_2 \in [q_1, 1.0]$, and that the halo orientation $\hat{\mathbf{n}}$ is random, we find $\Delta N = 0.085$.

Figure 2 shows the difference between the observed scatter and the Poisson expectation as a function of ΔN for three different richness clusters as labelled. The bias in the mean is very nearly zero, and is therefore not shown. Evidently, large ΔN values can contribute significantly to the observed scatter. For the expected level of halo-triaxiality (vertical dotted line), the impact of this effect on the richness–mass relation is border-line significant.

4.3. Cluster-to-Cluster Variance of Ridgeline Properties

In a recent work, Hao et al. (2009) found cluster-to-cluster variations of order 0.05 magnitudes in the mean color of ridgeline cluster galaxies at fixed redshift. Unfortunately, they did not determine whether such fluctuations were intrinsic, or simply reflected measurement error. If the former dominates, one needs to consider whether such intrinsic fluctuations could impact the richness–mass relation of galaxy clusters.

In our original simulations, the color of cluster galaxies is randomly drawn from a Gaussian distribution of mean \bar{c} and standard deviation $\sigma_c = 0.05$. We include variations in the properties of ridgeline galaxies by setting the mean color of cluster galaxies to $\bar{c} = \bar{c}_0 + \Delta c$ where \bar{c}_0 is the mean color of cluster galaxies over all clusters, and Δc is a random Gaussian color offset of zero mean and standard deviation $\sigma_{\bar{c}}$.

We find that the scatter in ridgeline properties has no impact on the mean or scatter of the richness–mass relation at the 1% level. This robustness reflects the fact that λ is not particularly sensitive to the precise location of the central peak in the color filter (see papers I and III for an extended discussion), so that small differences between the color distribution used to generate cluster galaxies and the actual filter employed in estimating cluster richness have only a modest impact on the final cluster richness estimate. This is also good news for the purposes of extending this work to higher redshifts, since any intrinsic cluster-to-cluster variation in the properties of ridgeline galaxies would likely increase with increasing redshift. In paper III, we explicitly consider the sensitivity of λ to the details of the red-sequence model. More specifically, we demonstrate that λ is robust to whether we employ our red-sequence model, or whether we empirically fit for the red-sequence parameters on a cluster-by-cluster basis. This is consistent with the analysis presented here that cluster-to-cluster variance in ridgeline properties is not an important source of scatter in the richness–mass relation.

4.4. Photometric Errors

Photometric errors impact a cluster’s richness estimate in two ways: they can scatter galaxies across the luminosity cut used to count galaxies, and they can scatter the location of a galaxy in color space. We test the impact of each of these effects in turn.

To include photometric errors in our simulations, we compute the median error $\sigma_i(i)$ and $\sigma_{g-r}(i)$ on i and $g-r$ as a function of i in the SDSS. For each galaxy in our simulation, we then set $i_{obs} = i_{true} + \Delta i$ where Δi is a random Gaussian offset of zero mean and standard deviation $\sigma_i(i_{true})$. Finally, the galaxy is assigned a photometric error $\sigma_i(i_{obs})$. A similar operation can be

performed with $g-r$. In order to disentangle the impact of photometric errors in i with those in $g-r$, we consider simulations in which i band magnitudes are subject to photometric errors, but $g-r$ is not, as well as the converse case.

We parameterize the photometric error function $\sigma_i(i)$ and $\sigma_{g-r}(i)$ as

$$\sigma_i(i) = \sigma_{i,20} \exp(0.56(i - 20)) \quad (16)$$

$$\sigma_{g-r}(i) = \sigma_{g-r,20} \exp(0.70(i - 20)). \quad (17)$$

The pivot point $i = 20$ is chosen simply as a convenient reference magnitude for galaxies at redshift $z \approx 0.25$ brighter than $0.2L_*$. These parameterization provide reasonable fits to the SDSS data. In our simulations, we vary the amplitude parameters in the range $\sigma_{i,20} \in [0, 0.2]$ and $\sigma_{g-r,20} \in [0, 0.4]$. The amplitudes in the SDSS are $\sigma_{i,20} = 0.04$ and $\sigma_{g-r,20} = 0.11$. We find that over the ranges probed — which extend significantly beyond the precision of SDSS photometry — photometric errors do not affect the scatter in richness–mass relation of galaxy clusters in a significant way. Not surprisingly, sufficiently large photometric errors can impact the mean cluster richness, but doing so requires a photometric uncertainty $\sigma_{i,20} \gtrsim 0.1$, significantly larger than the 0.04 error from SDSS. Thus, the photometric calibration in SDSS has a negligible impact on the richness–mass relation of galaxy clusters. This conclusion will only be strengthened in future surveys, where photometric uncertainties will be further reduced. This is also consistent with the tests we perform in paper III, where we demonstrate that λ is only modestly affected by errors of up to 0.05 magnitudes in the magnitude cut corresponding to our luminosity threshold.

4.5. Photometric Redshift Errors

Our richness estimate λ is the number of red-sequence galaxies brighter than a given luminosity cut and within a specified radial cut. However, the physical radial offset and luminosity of a galaxy depends on the cluster’s redshift, as does the color of the red-sequence. Consequently, scatter in a cluster’s redshift can produce scatter in the richness–mass relation. To test whether this is significant, we perform Monte Carlo realizations as described in section 3. We then assume that the cluster is assigned an observed redshift $z_{obs} = z_{true} + \Delta z$, where Δz is a random Gaussian offset of zero mean and standard deviation σ_z . The assigned luminosity of every galaxy is then rescaled by the square of the luminosity distance ratio between the true and observed redshift. The radial locations of the galaxies are also scaled by the angular diameter distance ratio. The cluster richness is then estimated as usual.

Figure 3 shows how the mean and scatter of the richness–mass relation depends on the standard deviation of the photometric redshift errors σ_z . What is remarkable about this figure is how fast redshift errors go from irrelevant to significant. Below $\sigma_z \approx 0.02$, photometric redshift errors are not very important, but their contribution to the total scatter rapidly increases with σ_z beyond this point. Thus, accurate photometric redshift estimates are necessary in order to avoid significantly increasing the scatter of the richness–mass relation. For reference, the photometric redshift accuracy of

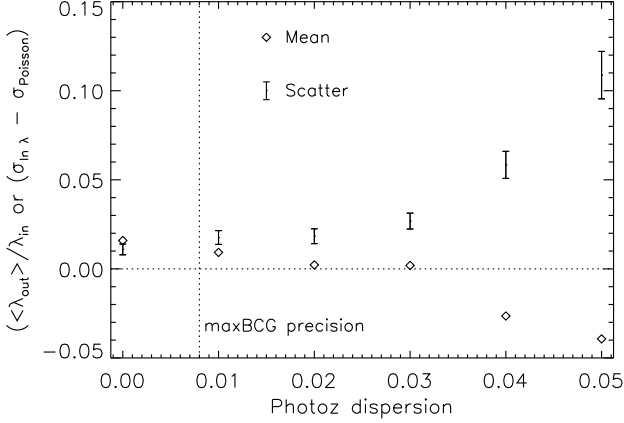


FIG. 3.— Mean and scatter of the richness–mass relation as a function of photometric redshift errors. Photometric redshift errors need to be controlled at the $\Delta z \lesssim 0.02$ level for them to have a negligible impact on the richness–mass relation. This value is comfortably above the estimated photometric redshift error of maxBCG clusters (vertical dotted line).

SDSS maxBCG clusters is $\sigma_z \approx 0.008$, so cluster photometric redshift errors are not a significant systematic in this case.

We can easily understand why photometric redshift errors can become so important so quickly. If one takes a galaxy at the median redshift of the cluster sample, and displaces it in redshift by Δz , the corresponding magnitude change is roughly $\Delta m = 10\Delta z$, so a redshift error of 0.02 changes the apparent luminosity of a cluster galaxy by 0.2 magnitudes, a relatively large amount. Moreover, unlike photometric errors, all galaxies step in unison, and the effect of this scatter is not down-weighted by root- N statistics.

The results of this section can also speak to the importance of uniform photometric calibration when characterizing the scatter in the richness–mass relation. As discussed above, a photometric redshift error of 0.02 corresponds to a photometric shift of 0.2 magnitudes; at this point, photometric redshift errors become important. Consequently, in order for the scatter of the richness–mass relation to remain unaffected by variations in the photometric calibration of a survey, the latter needs to be controlled at the level of 0.2 magnitudes.

4.6. Cluster Miscentering

We consider the impact that cluster miscentering — i.e. the possibility that the cluster center chosen by an observer may be offset from the true cluster center — can have on the richness–mass relation. We adopt the mis-centering parameterization used in Johnston et al. (2007) to characterize the centering properties of the maxBCG cluster-finding algorithm and explore how our richness measure depends on these quantities. The two parameters of interest are the probability p that a cluster be correctly centered, and the standard deviation σ_R characterizing the distribution of random offsets for mis-centered clusters (see below).

We incorporate mis-centering in our simulations as follows: for each cluster realization, we randomly determine whether the cluster is mis-centered or not based on its centering probability. If the cluster is mis-centered, we

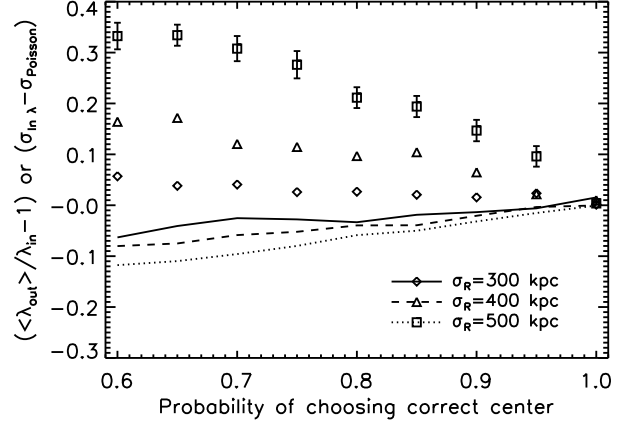


FIG. 4.— Mean and scatter of the richness–mass relation as a function of mis-centering parameters. Isolated symbols always track the scatter data, while the curves trace the mean data. The parameter σ_R is the standard deviation of the random displacement vector applied when clusters are mis-centered. Not surprisingly, mis-centering can severely impact both the mean and the scatter of the richness–mass relation if mis-centering offsets are comparable to the aperture used for estimating richness (1 Mpc in our simulations).

draw a random offset vector by randomly selecting a position angle, and then randomly sampling the offset along the corresponding axis from a Gaussian of zero mean and standard deviation σ_R . We then measure the richness λ about this new cluster center. Note that we are not enforcing the cluster center to fall on a cluster galaxy. This procedure allows us to vary the mis-centering parameters in a smooth fashion in order to explore the sensitivity of our results to the input parameters.

Figure 4 shows how the mean (curves) and scatter (symbols) of the richness–mass relation depends on the mis-centering parameters for a variety of σ_R values: $\sigma_R = 0.1$ Mpc (solid, diamonds), $\sigma_R = 0.3$ Mpc (dashed, triangles), and $\sigma_R = 0.5$ Mpc (dotted, squares). The horizontal axis is the probability p that a cluster be correctly centered. Not surprisingly, when the mis-centering offset parameter σ_R is comparable to the λ -aperture ($\sigma_R \gtrsim R_\lambda/2$), richnesses are systematically underestimated and the scatter of the richness–mass relation is dramatically increased. Importantly, however, notice that miscentering “turns-o” remarkably fast. For $p \approx 0.85$ and $\sigma_R/R \lesssim 0.4$, miscentering does not appear to be an important systematic, but setting $p \approx 0.75$ and $\sigma_R/R = 0.5$ significantly increases the scatter. This is an important feature that we will return to in Appendix B of paper III.

What does this imply for the scatter in richness at fixed mass for maxBCG clusters. At $N_{200} \approx 25$ (50), the miscentering parameter $p \approx 0.7$ (0.8) and $\sigma_R \approx 0.4 h^{-1} \text{Mpc} \approx 0.57 \text{ Mpc}$ (Johnston et al. 2007; Hilbert & White 2010). The richness $N_{200} = 25$ (50) corresponds roughly to $\lambda = 30$ (60). Using our optimal richness estimator, the corresponding apertures are $R_c = 1.1$ (1.3) Mpc, and therefore the ratio $\sigma_R/R_c \approx 0.5$ (0.4). Assuming intrinsic Poisson scatter, and using Figure 4, we expect the total scatter in richness to be $\sigma_{\ln \lambda|M} = 0.48(0.23)$ for $\lambda = 30$ (60). The corresponding scatter in mass at fixed richness is obtained by multiplying the the slope of the mass–richness relation, which we

estimate in paper III as $\alpha = 1.07$. Our final estimate for the scatter in mass at fixed richness for $\lambda = 30$ (60) is therefore $\sigma_{\ln M|\lambda} \approx 0.5$ (0.25). The scatter at $\lambda = 60$ matches very well with our estimated scatter in mass from Figure B10 in paper III, while the value obtained here for $\lambda = 30$ is somewhat higher than that in Figure B10. Importantly, for $\lambda \gtrsim 60$, the centering probability p increases relative to $\lambda = 60$, while σ_R/R_c decreases. Putting everything together, this suggests that miscentering of maxBCG clusters is important for clusters with $\lambda \gtrsim 60$, at which point miscentering “turns on”, and leads to an increased scatter as a function of richness as one moves down in λ . This feature is indeed observed in Figure B10. Note, however, that our estimate for the scatter in mass at $\lambda = 30$ is somewhat higher than that of Figure B10, which suggests our miscentering model has too many miscentered clusters at $\lambda = 30$, and/or the miscentering kernel is too large for these systems.

5. THE IMPACT OF PROJECTION EFFECTS ON THE RICHNESS–MASS RELATION

5.1. Projection Effects in High Density Regions

In section 4, the galaxy density of non-cluster galaxies was modeled as a uniform density field where the mean density was set to the mean galaxy density over the entire sky. In practice, however, clusters reside in high-density regions, so the mean local galaxy density of non-cluster galaxies $b_{\text{local}}(i, g-r)$ is enhanced relative to global average.

Figure 5 shows the ratio of the local galaxy density $b_{\text{local}}(i, g-r)$ to the global mean $\bar{b}(i, g-r)$ as a function of magnitude for red-sequence (diamonds) and non-red sequence (triangles) galaxies. The solid line is a fit to the red-sequence boost over the region $0.1L_* \leq L \leq L_*$. The local galaxy density is estimated by selecting the 2000 richest maxBCG clusters (as determined using the richness estimator of Rozo et al. 2009), and then stacking them in narrow redshift bins of width $z = z_0 \pm 0.01$. Within each stack, we compute the mean galaxy density in an annulus of inner radius $R_{\text{in}} = 1 h^{-1}\text{Mpc}$ and outer radius $R_{\text{max}} = 2 h^{-1}\text{Mpc}$. It is this galaxy density that we report as the local galaxy density $b_{\text{local}}(i, g-r)$. Our choice of annulus is meant to purposely overestimate the mean galaxy density of non-cluster galaxies, so that we may place a robust upper limit on the impact that this galaxy density boost can have on the richness–mass relation.

We use the best-fit model from Figure 5 as a new background model for our Monte Carlo simulations. The exact model is

$$b_{\text{model}}(i, g-r) = (1 + \langle B|i \rangle) \bar{b}(i, g-r) \quad (18)$$

where

$$\langle B|i \rangle = \langle B_{20} \rangle \exp(-0.95(i - 20)) \quad (19)$$

and $\langle B_{20} \rangle = 0.28$. Note that this model is fit over the luminosity range $[0.1L_*, L_*]$, but grows exponentially fast with $i - 20$. In practice, the maximum boost we observe is ≈ 3 , so we impose a ceiling at $\langle B|i \rangle = 3$ at very bright magnitudes. The value of the ceiling has little impact on our results.

We find that the impact of this galaxy density boost to the richness–mass relation is unimportant. The richness of galaxy clusters is boosted by an average of 1.5

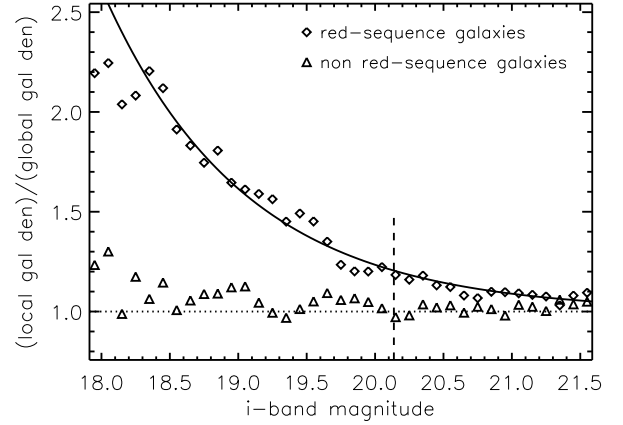


FIG. 5.— Ratio of the mean galaxy density in annuli around maxBCG clusters in the redshift range $z = [0.24, 0.26]$ to the mean galaxy density of the universe. We have split the galaxy sample into red-sequence and non red-sequence galaxies since the two populations show very different enhancements. The fact that the ratio is always larger than one illustrates that clusters reside in high density regions.

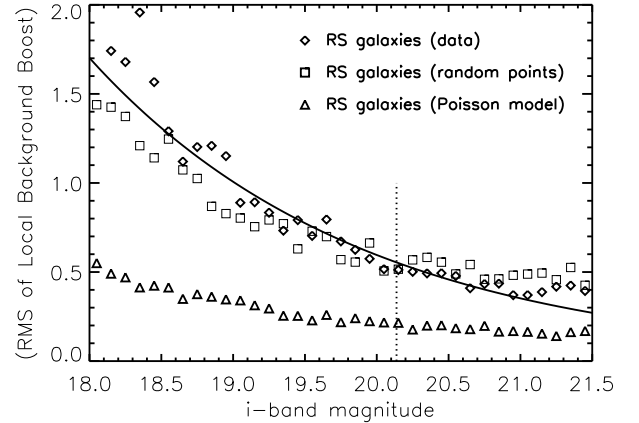


FIG. 6.— RMS fluctuations in the local background of red-sequence galaxies (diamonds) as a function of i -band magnitude for the redshift bin $z = [0.24, 0.26]$. The expected rms fluctuations from a Poisson model in which every cluster explores the same boosted background density field is shown with triangles, while the fluctuations of the local density about random points are shown as squares. The rms fluctuation in the local background is significantly larger than Poisson, signaling that cluster-to-cluster variations in the density of non-cluster galaxies is highly significant. Note, however, that these local fluctuations are only slightly larger than those about random points, implying that correlated structures around galaxy clusters do not dominate the variance in the local cluster background. The vertical dotted line corresponds to $0.2L_*$ at redshift $z = 0.25$.

galaxies, corresponding to a 3% bias for $\lambda = 50$ clusters. The scatter remains very nearly Poisson, with $\Delta\sigma_{\lambda_{\text{out}}} / \langle \lambda_{\text{out}} \rangle \approx 1.3\%$. These results are very sensible: the number of red-sequence galaxies within our chosen aperture around a random piece of sky is one to a few. Boosting this mean expectation by 30% can add one or two more non-cluster galaxies to the richness estimate, but not much more than that. Thus, the fact that the mean galaxy density near galaxy clusters is higher than the global average does not impact the richness–mass relation at a significant level.

Note, however, that a clustered background implies not only that the mean galaxy density around clusters is larger than the global average, but also that there can be cluster-to-cluster fluctuations in the background galaxy density. Figure 6 shows the rms fluctuations of the local background boost B of red-sequence galaxies (diamonds) along with a best-fit model (solid line). The rms fluctuations for blue galaxies are always smaller (not shown for clarity). In all cases, we estimate the rms fluctuation of the galaxy density field by estimating B as in the previous section using 100 bootstrap resamplings of the cluster catalog. Also shown for reference is the rms fluctuation of red-sequence galaxies about random points (squares), computed in the same way. Because the number of random points is significantly larger than the number of clusters available to us, one may worry that the additional variance we observe is simply due to measurement error rather than clustering. To test this hypothesis, we have measured the background fluctuations in Monte Carlo realizations from a model with a uniform boosted galaxy density, which are significantly smaller than those for the observed cluster population. Thus, we confirm that the galaxy density around galaxy clusters exhibits large cluster-to-cluster fluctuations.

We incorporate these cluster-to-cluster fluctuations in our background model by setting

$$b_{\text{model}}(i, g - r) = (1 + B(i))\bar{b}(i, g - r) \quad (20)$$

where B is now a random function. As in the previous section, we have ignored the color dependence of B , and we treat non red-sequence galaxies as red-sequence galaxies, which can only increase the impact of the variance of the density field. For simplicity, we also assume that the random fluctuations in B at different magnitudes are perfectly correlated, so that large overdensities of galaxies in one magnitude imply a large overdensity of galaxies at all magnitudes. Not only do we expect this to be physically reasonable, it should also maximize the relative importance of projection effects as opposite fluctuations at different magnitudes cannot cancel each other out. Our model for the function $B(i)$ is therefore

$$B(i) = \langle B|i \rangle + \frac{\Delta B(i)}{\Delta B_{20}} (B_{20} - \langle B_{20} \rangle) \quad (21)$$

where $\langle B|i \rangle$ and $\Delta B(i)$ are fits to the mean and standard deviation of the boost $B(i)$ of red-sequence galaxies observed in the data, and B_{20} is a random variable that determines the density boost of $i = 20$ red-sequence galaxies. The function $\langle B|i \rangle$ is again given by equation 19, while for the standard deviation we adopt

$$\Delta B(i) = \Delta B_{20} \exp[-0.52(i - 20)], \quad (22)$$

with $\Delta B_{20} = 0.60$ as in the data. The variable B_{20} in equation 21 is modeled as a log-normal random variable of the appropriate mean and standard deviation.

The solid histogram in Figure 7 shows the λ_{out} distribution of 10^4 realizations of a cluster with $\bar{\lambda}_{\text{in}} = 50$ with our lognormal local background model. The distribution is clearly peaked near the input value $\bar{\lambda}_{\text{in}}$, but is slightly biased, and exhibits a tail that extends to large λ values, which arise whenever the random background has an unusually large fluctuation due to random projection effects. Also shown as a solid curve is the best-fit Gaussian, where the fit is only performed over the region

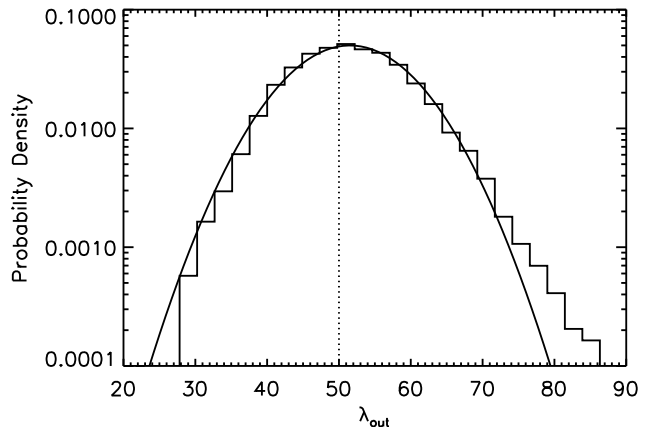


FIG. 7.— Richness distribution of a cluster of input richness $\bar{\lambda}_{\text{in}} = 50$ in the presence of local background fluctuations. The level of the local background fluctuations (both its mean and variance) has been set to the values measured in the SDSS data (see text for details). The dashed curve is a Gaussian fit to the region $\lambda_{\text{out}} \leq \bar{\lambda}_{\text{in}} + 2\bar{\lambda}_{\text{in}}^{1/3}$, which has a normalization constant $c = 0.99$, implying 99% of the cluster realizations have a scatter that is consistent with Poisson. The non-gaussian tails reflect rare occurrences where the background is boosted to very high levels due to random projection effects.

TABLE 1
PROPERTIES OF GAUSSIAN FIT TO $P(\lambda_{\text{out}}|\bar{\lambda}_{\text{in}})$

$\bar{\lambda}_{\text{in}}$	10	20	50	100
$1 - \langle \lambda_{\text{out}} \rangle / \bar{\lambda}_{\text{in}}$	13.0%	6.8%	3.2%	1.9%
$\langle \lambda_{\text{out}} \rangle - \bar{\lambda}_{\text{in}}$	1.3	1.4	1.6	1.9
$(\sigma_{\lambda_{\text{out}}} - \sigma_{\text{Poisson}}) / \langle \lambda_{\text{out}} \rangle$	2.8%	2.2%	1.0%	0.5%
c	95.2%	97.6%	98.9%	99.3%

^aHere, σ_{λ} is the standard deviation of λ , as opposed to the standard deviation of $\ln \lambda$, which we use throughout most of our work. The difference is simply to allow us to be formally correct when we quote the relative difference in terms of percentages in the table. The difference with respect to quoting $\Delta \sigma_{\ln \lambda}$ is insignificant.

$\lambda_{\text{out}} \leq \bar{\lambda}_{\text{in}} + 2\bar{\lambda}_{\text{in}}^{1/2}$ in order to prevent the tails of the distribution from affecting the fit. The best-fit parameters of the Gaussian are $\langle \lambda_{\text{out}} \rangle = 51.53 \pm 0.08$ and $\sigma_{\lambda_{\text{out}}} = 7.92 \pm 0.06$. Once again, we find a $\approx 3\%$ bias on the mean, while the width of the best-fit Gaussian remains close to the Poisson expectation ($\Delta \sigma_{\ln \lambda_{\text{out}}} = 1.4\%$). Importantly, however, the integral of the best-fit Gaussian is *not* unity. Defining c as the integral of the best-fit Gaussian, we find $c = 0.99$, implying that the tail of the distribution is formed by 1% of the clusters.

The results described above for a $\bar{\lambda}_{\text{in}} = 50$ clusters are generic. We have repeated this experiment using clusters with $\bar{\lambda}_{\text{in}} = 10, 20$, and 100 , and in all cases, $P(\lambda_{\text{out}}|\bar{\lambda}_{\text{in}})$ exhibited the same features: a main Gaussian peak whose mean is biased high, a width that is very close to the Poisson expectation, and a normalization constant c slightly less than unity. As one might expect, the impact of a stochastic background is smaller in richer systems. Table 1 summarizes those results.

5.2. Cosmological Interpretation

Our results paint a very clear picture of how projection effects operate in the real universe: for the vast major-

ity of halos — $\gtrsim 99\%$ at high mass and $\gtrsim 95\%$ at low mass (see table 1) — the density of non-cluster galaxies within the cluster field has a negligible impact on the richness estimate for the halo. In roughly $1\% - 5\%$ of all cases, however, the halo resides within a galaxy density field that is much denser than average, which results in a large contribution of non-halo galaxies to the richness estimate. That is, $\lesssim 5\%$ of all halos suffer from projection effects.

Interestingly, this is exactly the kind of picture that one should expect from CDM cosmologies. To see this, in the top and middle panels of Figure 8 we show the projected matter density in spheres of radius $R = 170$ Mpc around a random $10^{14} M_{\odot}$ (strictly speaking $M = 1.57 \times 10^{14} M_{\odot}$) halo in the Millenium Gas Simulation at $z=0$ — a GADGET-2-driven replica of the Millennium Simulation (Springel et al. 2005), where half of the one billion particles are treated as gas particles subject to hydrodynamics; for a further details see (Gazzola & Pearce 2006; Hartley et al. 2007; Stanek et al. 2010). The idea for these plots comes from the work of Colberg et al. (1999), who used these type of plots to understand the large scale structure about galaxy clusters (Colberg et al. 1999). The 170 Mpc radius is a very conservative estimate for the distance along the line of sight corresponding to the width of the red-sequence, and the gray scale is chosen so that darker regions correspond to higher densities, with the top panel being log-scale while the middle panel is linear.

These maps do not look qualitatively different when we use halos of higher and/or lower mass, nor when we vary R_{max} in the range 100 Mpc – 200 Mpc. Now, consider how an observer would see a cluster. The line of sight from the observer to the cluster pierces the density map at exactly one point. Because projection effects are linear in the density field, the middle panel in Figure 9 can be thought of as a map of the importance of projection effects. The fact that this middle panel is essentially empty reflects the fact that for a uniform line of sight sampling, most observers will see a cluster with no projections. Only a small subset of observers will severely overestimate the richness, as we argued based on empirical evidence.

This is best illustrated by the lower panel in Figure 8, which was constructed as follows. Starting from the projected density field, for any given pixel with density Σ_{pix} , we compute the fractional area of the sphere where $\Sigma \geq \Sigma_{pix}$. Thus, strong overdensities have $f \lesssim 1$, while strong underdensities have $f \approx 1$. In this way, we can remap the density field from the top and middle panels into a map of fractional area coverage. We see that the tight density knots from the top and middle panels cover only $\approx 1\%$ of the sphere, with filaments cover $\approx 10\%$ of the area, which is consistent with our empirical estimates of the fraction of galaxy clusters that suffer from severe projection effects.

One question that remains to be addressed is whether or not projection effects are dominated by local structures or uncorrelated structures. To address this question, we compare the variance of the local density field around galaxy clusters (Figure 6, diamonds) to the variance around random points in the sky (Figure 6, squares). If correlated structures dominate the variance of the density field, then the former will be significantly larger than the latter. However, this is not what we ob-



FIG. 8.— The projected surface matter density around a random $z = 0$, $M = 1.57 \times 10^{14} M_{\odot}$ halo in the Millenium simulation with gas (Springel et al. 2005; Gazzola & Pearce 2006). Only matter within a radius $R = 170$ Mpc of the halo is projected, corresponding to the 2σ interval spanned by the width of the red-sequence. The density scale is such that darker regions correspond to higher density, and is logarithmic in the top panel but linear in the middle panel. Projection effects are linear in the density field, and therefore the middle panel can be thought of as a map of how important local projection effects to that cluster are as a function of line of sight. Note most lines-of-sight fall in a white, empty space, for which projection effects are negligible. To better illustrate this, in the bottom panel we should the same density field, but now color coded according to the fractional area f , so that a pixel of density Σ_{pix} is assigned a value f that is the fraction of the sphere covered by pixels with $\Sigma \geq \Sigma_{pix}$. We see that all the dense knots from the top and middle panels cover only $\approx 1\%$ of the sphere, while the filamentary structure covers $\approx 10\%$. This illustrates that CDM cosmologies predict that most halos do not suffer from projection effects.

served, so we can conclude that while correlated structures certainly enhance projection effects, they are not overwhelmingly dominant.

It is difficult to say whether this last conclusion — that correlated structures do not necessarily dominate overall projection effects — generalizes to high redshift. On the one hand, it is expected that the width of the red-sequence will correspond to increasingly larger distances along the line of sight, which would tend to make uncorrelated structures more important. On the other hand, at fixed halo mass, higher redshift halos are rarer peaks, which would increase the relative importance of correlated structures. Given the relatively modest impact that correlated structures have at low redshift, however, we would be surprised if projection effects from uncorrelated structure ever becomes negligible.

5.3. Projection Effects, and Their Implication for Completeness and Purity

When interpreting our results, it is also important to distinguish the fraction of *halos* that suffer from projections effects, from the fraction of *optically selected clusters* that suffer from projection effects. Specifically, due to the steepness of the halo mass function, the frequency of optically selected clusters that suffer from projection effects will be higher, as at any richness there are always more low mass halos scattering in and than out. To estimate this effect, we proceed as follows. First, we measure the richness λ of every cluster in the maxBCG cluster catalog (Koester et al. 2007), and fit the corresponding abundance function as a power-law, restricting ourselves to the richness range $30 \leq \lambda \leq 60$.¹¹ We then select a fraction $1 - c(\lambda)$ of the clusters (as measured from our simulations), boost their richness as described below, and recompute the richness function. The difference between the original and boosted abundances gives the fraction of clusters that suffer from projection effects. We denote this fraction $p(\lambda)$, and refer to it as the purity. For $c(\lambda)$, we fit the data in table 1 to find

$$c(\lambda) = 1 - 0.014(\lambda/40)^{-0.84}. \quad (23)$$

We consider three distinct methods for boosting the abundance of galaxy clusters, corresponding to an optimistic, a pessimistic scenario, and a super-pessimistic scenario. In the pessimistic scenario, we assume a halo of richness λ is projected onto another halo of richness λ , so the boosted richness becomes 2λ . This is pessimistic in that for unequal richness projections, the richer of the two objects can always be considered the main halo. The super-pessimistic scenario is as the pessimistic scenario, but we double the number of halos that suffer from projection effects. In the optimistic case, we simply demand that the projection effects be larger than Poisson fluctuations, so we set the boosted richness to $\lambda + 2\lambda^{1/2}$. i.e. projection effects only increase the richness by twice the standard deviation from Poisson statistics. The motivation for relying on these simple models rather than our Monte Carlo simulations is that our simulations are almost certainly not correct in detail, but these analytic arguments should bracket the correct answer.

Figure 9 shows the purity function for our three models. At high richness ($\lambda \gtrsim 40$), the purity remains high

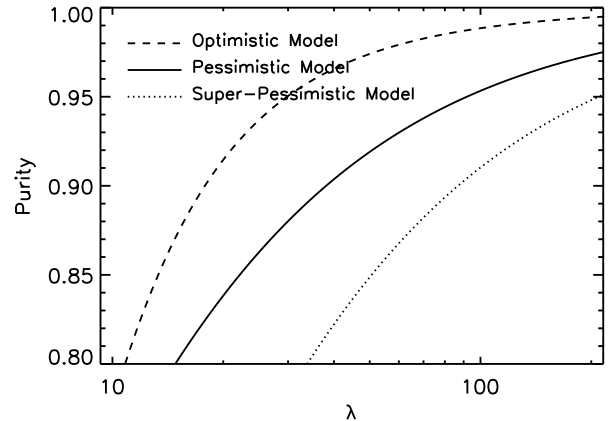


FIG. 9.— The predicted purity of the optically selected cluster as a function of the richness λ . By purity, we mean the fraction of clusters of richness λ that do *not* suffer from projection effects. This quantity is computed using two simple models for projection effects, an optimistic model (dashed) and a pessimistic one (solid). The true impact of projection effects is likely to fall somewhere in between the two lines, and probably closer to our optimistic model. Thus, a reasonably value for the fraction of clusters that do not suffer from projection effects for $\lambda \approx 30$ is $p = 90\%$.

($p \gtrsim 0.9$), but quickly decreases with decreasing richness. Note that by ignoring the curvature of the richness function, we are somewhat over-estimating the purity in the high richness range, and under-estimating the purity in the low richness range. In light of these considerations and the simple analytic nature of our model, a reasonable value for the purity function is $p \approx 90\%(95\%)$ at $\lambda = 30$ (100).

5.4. Discussion

Our results in this section are most directly comparable to the work of Cohn et al. (2007) (though see also Cohn & White 2009; Noh & Cohn 2011) who relied on N-body simulations to explore the impact of local structures on richness estimates. Their work is highly complementary to ours: N-body simulations provide a very realistic treatment of correlated structures, whereas relying on Monte Carlo realizations of simple analytic models allows us to generate many thousands of cluster realizations with varying sources of error, a flexibility that was a necessary component of the study we undertook. It should also be noted that the work of Cohn et al. (2007) differs from ours in that they employed a different richness estimator that is specifically tuned to their simulation, and, as noted earlier, such details will have a quantitative impact on our results. Despite all these differences, the two results reach similar conclusions, with Cohn et al. (2007) estimating that local projection effects are important for $\lesssim 10\%$ of all optically selected clusters.

It is not too surprising that this is the case. To see this, we note that the density boost due to cluster environment satisfies $\Delta B > \langle B \rangle \approx 0$. The only way that this condition can be satisfied given the constraint $B > 0$ is if the probability distribution $\rho(B)$ is sharply peaked near $B \approx 0$, but has tails extending to large values of B . As long as the tail is pronounced, differences in how one estimates the fraction of objects in the tail will have little impact on the results.

¹¹ Here, λ is measured as detailed in paper III, rather than using the simpler filters employed in this work. Over the range of richness we consider, however, the two agree well. We are not concerned about the detailed differences since our goal here is only to provide a rough estimate of projection effects.

Finally, we discuss the consequences of this work for the classic purity and completeness tests that are often applied to evaluate optical cluster finding algorithms. The basic idea in these tests is this: to test completeness and purity, one takes the survey area, and randomizes the position and/or color of every galaxy in the survey. By embedding galaxy clusters at known positions and redshifts within the shuffled sky map, one can estimate both purity and completeness.

There are multiple problems with the test we just described. First, randomizing galaxy positions (e.g. Postman et al. 1996; Kepner et al. 1999) is equivalent to setting the background galaxy density to a uniform density field, which results in effectively no projection effects. An alternative possibility is to randomize galaxy colors while holding galaxy positions fixed or minimally displaced (e.g. Goto et al. 2002; Koester et al. 2007; Bellagamba et al. 2010), but we have seen that blue galaxies are significantly less structured than red galaxies, so once again this is not adequate.

The insight developed in this paper allows one to easily modify these tests to avoid such difficulties. In particular, given that projection effects by non-correlated structures appear to be at least comparable to projection effects from correlated structures, we expect that simply placing clusters in random points of the sky *without galaxy position and color randomization* should be a significantly more realistic test of cluster completeness and the impact of projection effects (this is similar to the approach adopted in Wen et al. 2009b). That said, such a test would still ignore the slight boost to the mean and variance of the density field near clusters. To fix this, one could simply displace every cluster by two or three cluster radii, and re-estimate its richness. Based on our results, we expect this to be a significantly better test for evaluating the performance of cluster-finding algorithms. Note that when performing such a test, one will occasionally displace one cluster on top of another. That is precisely the point: this type of overlap occurs in reality, so enforcing that clusters not be displaced on top of one another, as is sometimes done, would lead to an under-estimate of projection effects.

Of course, one might wonder whether such tests are even necessary in the advent of large N-body simulations that can be populated with galaxies in ways that accurately reflect the known universe (see eg. Miller et al. 2005; Rozo et al. 2007b; Dong et al. 2008; Milkeraitis et al. 2010, for works that have relied on numerical simulations to calibrate cluster selection). While such simulations are invaluable, and have, in fact, led to many improvements in our understanding of optical cluster selection, the development of tests that can be applied on both on real and simulated data sets have the potential of being of critical importance. Specifically, if various systematics can be calibrated directly from the data using these empirically driven tests, then one can use simulations to test the efficacy of these methods rather than having to rely on simulations for calibration purposes, which can introduce additional systematic uncertainties that are difficult to quantify.

6. SUMMARY

We have used Monte Carlo simulations to explore various possible sources of *extrinsic* scatter of the richness–

mass relation in order to identify which, if any, are non-negligible. By “negligible”, we mean that the source of noise under consideration does not increase the scatter of the richness–mass relation by more than 5% relative to the Poisson expectation. This criterion is motivated by the precision required to robustly estimate cosmological parameters in a DES-like survey (see Appendix A).

We find that cluster-to-cluster variance in the properties of ridgeline galaxies, photometric errors, and photometric redshift errors are all negligible. Cluster triaxiality is border-line significant, increasing the scatter of the richness–mass relation by $\sim 5\%$ in the richest systems. The most significant source of extrinsic scatter by far is cluster miscentering, though the details of the effect depends on the model parameters assumed. Using the Johnston et al. (2007) miscentering model, which is consistent with weak lensing observations (Oguri et al. 2010), we find that miscentering is likely to be significant for $\lambda \lesssim 60$, but less so above this limit. The total scatter from Poisson noise plus miscentering is close to the empirically estimated scatter in Appendix B of paper III at $\lambda \approx 60$, but appears to over-estimate the scatter by $\lambda \approx 30$, suggests that the miscentering model we considered over-estimates the importance of cluster miscentering at low richness. It is clear, however, that miscentering is likely to play an important role in the richness–mass relation, particularly at low masses.

Finally, we considered the impact of projection effects on the richness–mass relation for a variety of assumptions about the environment of galaxy clusters. As one might expect, we find that clustering of the background density field plays an important role on projection effects. Less obvious however is that the boost to the mean galaxy density around a cluster is unimportant. Rather, projection effects are sourced by large cluster-to-cluster fluctuations in the background galaxy density. Having estimated the variance of the background density field directly from SDSS data, we demonstrated that a small fraction of halos ($\approx 1\% - 5\%$) are expected to suffer from severe projection effects. Due to the steepness of the mass function, the relative fraction of optically selected clusters that suffer from projection effects is higher, roughly i.e., $\sim 5\% - 15\%$. *We emphasize that all these results are obtained using empirically motivated assumptions.* We also demonstrated that these results arise naturally in CDM cosmologies, and, indeed, our results are consistent with those Cohn et al. (2007), who relied on N-body simulations to answer similar questions.

Our results have important consequences for the classical purity and completeness tests used to test optical cluster-finders. Specifically, we demonstrated that simply randomizing the positions of galaxies in the sky and then inserting galaxy clusters will grossly underestimate the importance of projection effects. A much better test is simply to place the clusters at random points in the sky without galaxy randomization, or, even better, to simply displace clusters by two to three cluster radii and then to re-estimate their richness. Most importantly, if such displacements lead to overlapping clusters, one should keep those realizations, as such alignments naturally occur in the data set.

Overall, we believe the results from this work are very encouraging. Between papers I and III, we believe we have considered all major modifications that could be

made to our richness estimator. Consequently, we are confident our final estimator is very close to optimal. In addition, paper III also demonstrates that our estimator is extremely robust. With this work, we have developed a thorough qualitative understanding of the sources of noise that can significantly impact the scatter of the richness–mass relation, and we have also been able to identify the most important observational systematic, namely miscentering. Importantly, miscentering is not a problem of the richness estimator, but rather one having to do with cluster finding: i.e. one needs to know how to adequately center clusters, a question that we have not addressed in this work. Finally, we believe we have provided solid empirical evidence in favor of projection effects in galaxy clusters being a relatively mild effect, and what’s more, an effect that can be empirically calibrated. We intend to return to the question of how to model all these effects quantitatively in a future paper.

All in all, we think these results justify being hopeful about our ability to optimize cluster richness estimation for upcoming photometric cluster surveys, such as DES and LSST.

ER would like to thank Joanne Cohn, Matthew Becker, and Andrey Kravtsov for helpful discussions and suggestions about the content of this manuscript. ER is funded by NASA through the Einstein Fellowship Program, grant PF9-00068. ESR thanks the TABASGO foundation. A.E.E. acknowledges support from NSF AST-0708150 and NASA NNX07AN58G. RHW and HW received supported from the DOE under contract DE-AC03-76SF00515. This work was supported in part by the Director, Office of Science, Office of High Energy and Nuclear Physics, of the U.S. Department of Energy under Contract No. AC02-05CH11231.

REFERENCES

- Allgood, B., Flores, R. A., Primack, J. R., Kravtsov, A. V., Wechsler, R. H., Faltenbacher, A., & Bullock, J. S. 2006, *MNRAS*, 367, 1781
- Bartelmann, M. 1996, *A&A*, 313, 697
- Bellagamba, F., Maturi, M., Hamana, T., Meneghetti, M., Miyazaki, S., & Moscardini, L. 2010, *ArXiv e-prints*
- Berlind, A. A., Weinberg, D. H., Benson, A. J., Baugh, C. M., Cole, S., Davé, R., Frenk, C. S., Jenkins, A., Katz, N., & Lacey, C. G. 2003, *ApJ*, 593, 1
- Bett, P., Eke, V., Frenk, C. S., Jenkins, A., Helly, J., & Navarro, J. 2007, *MNRAS*, 376, 215
- Blake, C., Collister, A., & Lahav, O. 2008, *MNRAS*, 385, 1257
- Boylan-Kolchin, M., Springel, V., White, S. D. M., & Jenkins, A. 2010, *MNRAS*, 406, 896
- Busha, M. T., Wechsler, R. H., Behroozi, P. S., Gerke, B. F., Klypin, A. A., & Primack, J. R. 2010, *ArXiv e-prints*
- Cohn, J. D., Evrard, A. E., White, M., Croton, D., & Ellingson, E. 2007, *MNRAS*, 382, 1738
- Cohn, J. D. & White, M. 2009, *MNRAS*, 393, 393
- Colberg, J. M., White, S. D. M., Jenkins, A., & Pearce, F. R. 1999, *MNRAS*, 308, 593
- Cunha, C., Huterer, D., & Frieman, J. A. 2009, *Phys. Rev. D*, 80, 063532
- Dong, F., Pierpaoli, E., Gunn, J. E., & Wechsler, R. H. 2008, *ApJ*, 676, 868
- Eisenstein, D. J., Annis, J., Gunn, J. E., Szalay, A. S., Connolly, A. J., Nichol, R. C., Bahcall, N. A., Bernardi, M., Burles, S., Castander, F. J., Fukugita, M., Hogg, D. W., Ivezić, Ž., Knapp, G. R., Lupton, R. H., Narayanan, V., Postman, M., Reichart, D. E., Richmond, M., Schneider, D. P., Schlegel, D. J., Strauss, M. A., SubbaRao, M., Tucker, D. L., Vanden Berk, D., Vogeley, M. S., Weinberg, D. H., & Yanny, B. 2001, *AJ*, 122, 2267
- Evrard, A. E. 1989, *ApJ*, 341, L71
- Gazzola, L. & Pearce, F. R. 2006, *arXiv, astro-ph*
- Gladders, M. D. & Yee, H. K. C. 2000, *AJ*, 120, 2148
- Goto, T., Sekiguchi, M., Nichol, R. C., Bahcall, N. A., Kim, R. S. J., Annis, J., Ivezić, Ž., Brinkmann, J., Hennessy, G. S., Szokoly, G. P., & Tucker, D. L. 2002, *AJ*, 123, 1807
- Hansen, S. M., Sheldon, E. S., Wechsler, R. H., & Koester, B. P. 2007, *ArXiv e-prints*, 710
- Hao, J., Koester, B. P., McKay, T. A., Rykoff, E. S., Rozo, E., Evrard, A., Annis, J., Becker, M., Busha, M., Gerdes, D., Johnston, D. E., Sheldon, E., & Wechsler, R. H. 2009, *ApJ*, 702, 745
- Hao, J., McKay, T. A., Koester, B. P., Rykoff, E. S., Rozo, E., Annis, J., Wechsler, R. H., Evrard, A., Siegel, S. R., Becker, M., Busha, M., Gerdes, D., Johnston, D. E., & Sheldon, E. 2010, *ApJS*, 191, 254
- Hartley, W. G., Gazzola, L., Pearce, F. R., Kay, S. T., & Thomas, P. A. 2007, *arXiv, astro-ph*, 8 pages, 7 figures, submitted to *MNRAS*
- Hilbert, S. & White, S. D. M. 2010, *MNRAS*, 404, 486
- Hockney, R. W. & Eastwood, J. W. 1981, *Computer Simulation Using Particles* (Computer Simulation Using Particles, New York: McGraw-Hill, 1981)
- Jing, Y. P. & Suto, Y. 2002, *ApJ*, 574, 538
- Johnston, D. E., Sheldon, E. S., Wechsler, R. H., Rozo, E., Koester, B. P., Frieman, J. A., McKay, T. A., Evrard, A. E., Becker, M. R., & Annis, J. 2007, *ArXiv:0709.1159*
- Kasun, S. F. & Evrard, A. E. 2005, *ApJ*, 629, 781
- Kepner, J., Fan, X., Bahcall, N., Gunn, J., Lupton, R., & Xu, G. 1999, *ApJ*, 517, 78
- Knebe, A. & Wielebner, V. 2006, *Publications of the Astronomical Society of Australia*, 23, 125
- Kochanek, C. S., White, M., Huchra, J., Macri, L., Jarrett, T. H., Schneider, S. E., & Mader, J. 2003, *ApJ*, 585, 161
- Koester, B. P., McKay, T. A., Annis, J., Wechsler, R. H., Evrard, A. E., Rozo, E., Bleem, L., Sheldon, E. S., & Johnston, D. 2007, *ApJ*, 660, 221
- Koester et al. 2007, *ApJ*, 660, 239
- Kravtsov, A. V., Berlind, A. A., Wechsler, R. H., Klypin, A. A., Gottlöber, S., Allgood, B., & Primack, J. R. 2004, *ApJ*, 609, 35
- Milkeraitis, M., van Waerbeke, L., Heymans, C., Hildebrandt, H., Dietrich, J. P., & Erben, T. 2010, *MNRAS*, 406, 673
- Miller, C. J., Nichol, R. C., Reichart, D., Wechsler, R. H., Evrard, A. E., Annis, J., McKay, T. A., Bahcall, N. A., Bernardi, M., Boehringer, H., Connolly, A. J., Goto, T., Kniazev, A., Lamb, D., Postman, M., Schneider, D. P., Sheth, R. K., & Voges, W. 2005, *AJ*, 130, 968
- Navarro, J. F., Frenk, C. S., & White, S. D. M. 1995, *MNRAS*, 275, 56
- Noh, Y. & Cohn, J. D. 2011, *MNRAS*, 158
- Oguri, M., Takada, M., Okabe, N., & Smith, G. P. 2010, *MNRAS*, 405, 2215
- Peebles, P. J. E., Daly, R. A., & Juszkwicz, R. 1989, *ApJ*, 347, 563
- Postman, M., Lubin, L. M., Gunn, J. E., Oke, J. B., Hoessel, J. G., Schneider, D. P., & Christensen, J. A. 1996, *AJ*, 111, 615
- Rozo, E., Chen, J., & Zentner, A. R. 2007a, *ArXiv e-prints* 0710.1683
- Rozo, E., Rykoff, E. S., Koester, B. P., McKay, T., Hao, J., Evrard, A., Wechsler, R. H., Hansen, S., Sheldon, E., Johnston, D., Becker, M., Annis, J., Bleem, L., & Scranton, R. 2009, *ApJ*, 703, 601
- Rozo, E., Wechsler, R. H., Koester, B. P., Evrard, A. E., & McKay, T. A. 2007b, *ArXiv Astrophysics e-prints, astro-ph/0703574*
- Rykoff, E., Koester, B., & Rozo, E. 2010, *ArXiv e-prints*
- Shapiro, C., Dodelson, S., Hoyle, B., Samushia, L., & Flaugher, B. 2010, *Phys. Rev. D*, 82, 043520
- Shaw, L. D., Weller, J., Ostriker, J. P., & Bode, P. 2006, *ApJ*, 646, 815
- Springel, V., White, S. D. M., Jenkins, A., Frenk, C. S., Yoshida, N., Gao, L., Navarro, J., Thacker, R., Croton, D., Helly, J., Peacock, J. A., Cole, S., Thomas, P., Couchman, H., Evrard, A., Colberg, J., & Pearce, F. 2005, *Nature*, 435, 629

- Stanek, R., Rasia, E., Evrard, A. E., Pearce, F., & Gazzola, L. 2010, *The Astrophysical Journal*, 715, 1508
- Strauss, M. A., Weinberg, D. H., Lupton, R. H., Narayanan, V. K., Annis, J., Bernardi, M., Blanton, M., Burles, S., Connolly, A. J., Dalcanton, J., Doi, M., Eisenstein, D., Frieman, J. A., Fukugita, M., Gunn, J. E., Ivezić, Ž., Kent, S., Kim, R. S. J., Knapp, G. R., Kron, R. G., Munn, J. A., Newberg, H. J., Nichol, R. C., Okamura, S., Quinn, T. R., Richmond, M. W., Schlegel, D. J., Shimasaku, K., SubbaRao, M., Szalay, A. S., Vanden Berk, D., Vogeley, M. S., Yanny, B., Yasuda, N., York, D. G., & Zehavi, I. 2002, *AJ*, 124, 1810
- Tinker, J. L., Wechsler, R. H., & Zheng, Z. 2010, *ApJ*, 709, 67
- Wen, Z. L., Han, J. L., & Liu, F. S. 2009a, *ApJS*, 183, 197
- . 2009b, *ApJS*, 183, 197
- Wetzel, A. R. & White, M. 2010, *MNRAS*, 403, 1072
- White, M. & Kochanek, C. S. 2002, *ApJ*, 574, 24
- Wu, H.-Y., Rozo, E., & Wechsler, R. H. 2008, *ApJ*, 688, 729
- Zehavi, I., Zheng, Z., Weinberg, D. H., Blanton, M. R., Bahcall, N. A., Berlind, A. A., Brinkmann, J., Frieman, J. A., Gunn, J. E., Lupton, R. H., Nichol, R. C., Percival, W. J., Schneider, D. P., Skibba, R. A., Strauss, M. A., Tegmark, M., & York, D. G. 2010, *ArXiv e-prints*
- Zheng, Z., Berlind, A. A., Weinberg, D. H., Benson, A. J., Baugh, C. M., Cole, S., Davé, R., Frenk, C. S., Katz, N., & Lacey, C. G. 2005, *ApJ*, 633, 791
- Zheng, Z., Zehavi, I., Eisenstein, D. J., Weinberg, D. H., & Jing, Y. P. 2009, *ApJ*, 707, 554

APPENDIX

HOW PRECISELY MUST THE SCATTER BE KNOWN IN A CLUSTER COUNTING EXPERIMENT?

We wish to quantitatively define when a source of scatter is observationally relevant. To do so, let us assume that the total scatter in the richness–mass relation of galaxy clusters is σ_{tot} , and that one performs a cosmological analysis of cluster abundance data in which the model scatter $\sigma_{model} \neq \sigma_{tot}$. Such an analysis will recover biased cosmological parameters, with the bias depending on the difference between σ_{tot} and σ_{model} . Of course, if these biases are small relative to the statistical uncertainties in the experiment, then they are not observationally relevant. Here, we consider deviations of the total scatter σ_{tot} from the model scatter σ_{model} where the model scatter is Poisson, and the total scatter includes extrinsic sources of scatter such as those considered in the main body of this work.

We address this problem within the context of a DES-like cluster cosmology experiment. For our fiducial survey, we assume a survey area of 5000 deg^2 , split into cells of 10 deg^2 area each, and a cluster selection threshold $M_{obs} \geq 7 \times 10^{13} M_{\odot}$ over a redshift range $0 \leq z \leq 1$. We further assume the cluster sample is binned in mass bins of width $\pm \Delta \log_{10} M_{obs} = 0.1$, corresponding to 5 bins per decade in mass, and we adopt a log-normal model for $M_{obs} - M_{true}$ relation, with

$$\langle \ln M_{obs} | M_{true} \rangle = a + b \ln M_{true} + c \ln(1 + z) \quad (\text{A1})$$

$$\sigma_{\ln M_{obs} | M_{true}} = \text{constant} = \sigma_{true}. \quad (\text{A2})$$

We assume both M_{true} and M_{obs} are measured in units of $7 \times 10^{13} M_{\odot}$, and set as our fiducial parameters $a = c = 0$ and $b = 1$.

Using the Fisher matrix technique described in detail in Wu et al. (2008), we then estimate what the cosmological constraints derived from our fiducial cluster sample would look like, assuming that the data is analyzed using the standard self-calibration technique, and that the scatter is fixed a priori to a known value σ_{model} . We do not, however, enforce that σ_{model} be identical to σ_{true} . Indeed, for any cosmological parameter p , the two most important numbers that come out of the Wu et al. (2008) Fisher matrix analysis are: a) the offset $\Delta p = p_{obs} - p_{true}$ between the recovered value of the cosmological parameter p and its true value, and b) the estimated statistical uncertainty $\sigma(p)$. Thus, given any combination of σ_{true} and σ_{model} , we can estimate the ratio $\Delta p / \sigma(p)$, and determine whether the difference between σ_{true} and σ_{model} is observationally relevant or not.

Figure A1 shows contours of the ratio $\Delta p / \sigma(p)$ for the dark energy parameters w_0 and w_a as a function of the scatter σ_{true} , and the a priori scatter value σ_{model} employed in the cosmological analysis. As is to be expected, the ratio $\Delta p / \sigma(p)$ goes to zero as $\sigma_{model} \rightarrow \sigma_{true}$, and increases as the difference between these two quantities increases. The two diagonal dash lines mark the equalities $\sigma_{model} = \sigma_{true} \pm 0.05$. As we can see, as long as σ_{model} is within about 0.05 of the true scatter σ_{true} , then the ratio $\Delta p / \sigma(p) \lesssim 0.5$ for both w_0 and w_a . In light of these considerations, we define an extrinsic source of noise as observationally relevant as one for which $\sigma_{true} - \sigma_{model} \geq 0.05$.

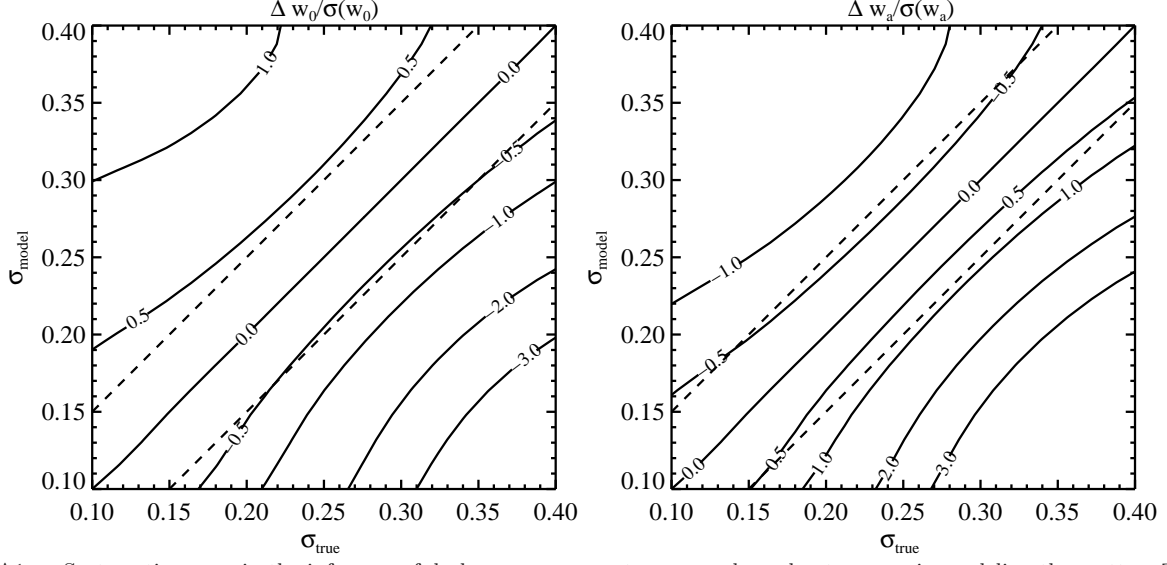


FIG. A1.— Systematic errors in the inference of dark energy parameters w_0 and w_a due to errors in modeling the scatter. The contours and numbers show the systematic errors Δw_0 (Δw_a) compared with statistical errors $\sigma(w_0)$ ($\sigma(w_a)$). The y-axis σ_{model} indicates the scatter value we use in the analysis, while the x-axis σ_{true} indicates the underlying true scatter. As can be seen, if $\sigma_{true} - \sigma_{model} \geq 0.05$, the recovered dark energy parameters will be significantly biased.